Micro-scale Mechanical Metamaterial with a Controllable Transition in the Poisson's Ratio and Band Gap Formation

*Krzysztof K. Dudek, Julio A. Iglesias Martínez, Gwenn Ulliac, Laurent Hirsinger, Lianchao Wang, Vincent Laude, Muamer Kadic**

K. K. Dudek, J. A. Iglesias Martínez, G. Ulliac, L. Hirsinger, L. Wang, V. Laude, M. Kadic
Institut FEMTO-ST, CNRS, Université Bourgogne Franche-Comté, Besançon 25030, France
K. K. Dudek
Institute of Physics, University of Zielona Gora, ul. Szafrana 4a, 65-069 Zielona Gora, Poland
Email Address: muamer.kadic@femto-st.fr

Keywords: *Mechanical Metamaterials, Auxetics, Micro-scale, Phonons, Band-gaps, Stimuli-responsive*

The ability to significantly change the mechanical and wave propagation properties of a structure without rebuilding it is currently one of the main challenges in the field of mechanical metamaterials. This stems from the enormous appeal that such tunable behavior may offer from the perspective of applications ranging from biomedical to protective devices, particularly in the case of micro-scale systems. In this work, a novel micro-scale mechanical metamaterial is proposed that can undergo a transition from one type of configuration to another, with one configuration having a very negative Poisson's ratio, corresponding to strong auxeticity, and the other having a highly positive Poisson's ratio. The formation of phononic band gaps can also be controlled concurrently which can be very useful for the design of vibration dampers and sensors. Finally, it is experimentally shown that the reconfiguration process can be induced and controlled remotely through application of a magnetic field by using appropriately distributed magnetic inclusions.

1 Introduction

Over the years, the importance of functional materials [1, 2, 3, 4, 5, 6, 7, 8, 9, 10, 11] has increased rapidly in our everyday lives. Most prominently in the span of the last two decades, different classes of these structures have been successfully implemented in numerous industries including biomedical [12, 13] and protective devices [14, 15, 16], sports equipment [17] as well as electronics [18, 19]. One of the most promising fields of study relating to such easily-applicable functional materials is that of mechanical metamaterials [20, 21, 22, 23, 24, 25, 26, 27, 28, 29, 30, 31, 32, 33, 34, 35, 36, 37]. Mechanical metamaterials are rationally designed structures that can exhibit counterintuitive mechanical properties based primarily on their design rather than their chemical composition. The most studied cases and well-known examples of metamaterials with extraordinary mechanical properties pertain to those with negative properties such as a negative Poisson's ratio (auxetic behavior) [20, 38, 39, 40, 41], negative stiffness [42, 43, 44, 45] and negative compressibility [42, 46, 47, 48]. Most notably, auxetic mechanical metamaterials have been proven to exhibit superior indentation resistance [49], energy absorption [50, 51] and wave attenuation [14, 52] in comparison to many conventional non-auxetic materials. However, despite the numerous advantages offered by mechanical metamaterials characterized by a negative value of Poisson's ratio, the vast majority of such structures share an important limitation. Namely, once typical auxetic metamaterials are manufactured, it is very difficult to change their mechanical characteristics without rebuilding the system. This, in turn, diminishes their applicability in fields where a variable response of the material is required. Nevertheless, as reported in recent years, this shortcoming can be addressed by the use of active mechanical metamaterials in the form of stimuli responsive structures.

Active mechanical metamaterials are structures that can exhibit a tunable mechanical behavior which depends on the application of an external stimulus. In recent years, it has been demonstrated that in the case of multi-material structures, the mechanical properties of the system can be adjusted remotely in a process that does not require reconstruction of the system. In the case of macroscopic systems, one of the most promising approaches used corresponds to the use of appropriately distributed inclusions in a form of magnets that respond to the application of an external magnetic field [53, 54]. However, this task becomes much more challenging at small scales. In these cases, one of the more feasible approaches which may be used is to utilise composite materials incorporating magnetic nanoparticles dis-

persed within a non-magnetic matrix [10, 55, 56, 57]. Another possible approach involves the use of several materials with different thermal expansion coefficients. In such a case, the behavior of the structure can be modified by changing the external temperature [56, 58]. This method, however, often does not allow one to obtain a very significant variation in the mechanical properties. In addition, the corresponding reconfiguration process tends to be quite slow. Last but not least, it is worth noting that it is possible to construct an active metamaterial composed of only one type of residual material that, to some extent, can undergo a change in its mechanical properties with a deformation pattern based solely on the variation of the mechanical stimulus, e.g. the rate of mechanical compression. A prime example of this approach corresponds to hierarchical metamaterials [59, 60, 61, 62, 63, 64, 65], where different hierarchical levels can deform independently of each other.

Despite several notable achievements, studies devoted to active mechanical metamaterials are still in their infancy and a far more in-depth analysis is required to fully harness their potential. First of all, it is important to emphasize that for a significant number of known active mechanical metamaterials, although it is possible to change one of their properties without rebuilding the system; this is very difficult to achieve whilst retaining control over the other properties. This problem is exacerbated further at small scales, such as the micro-scale, where the manufacturing process is often not only very difficult but also fairly expensive. On the other hand, despite these challenges, the ability to achieve simultaneous tunable control over multiple properties of a micro-scale system without the need for reconstruction is a very appealing concept that could be utilized in fields such as programmable robotics, vibration dampers / sensors and effective biomedical devices. In fact, in the literature [66], there are some rare examples demonstrating the possibility of simultaneously controlling several properties of micro-scale mechanical metamaterials. Some of the most promising studies describe the possibility of controlling Poisson's ratio [64] as well as wave propagation properties with an emphasis on tunable band gap formation [52, 67, 68]. However, despite their numerous advantages, such studies typically focus on complex hierarchical structures where the deformation process is not easily recoverable nor controlled due to the presence of multiple independently-deforming hierarchical levels. Furthermore, in most cases, it is also not possible to observe a large tunable change in the Poisson's ratio of the system, which significantly decreases the applicability of these systems.

In this work, a novel mechanical metamaterial is proposed that can be defined in the form of two distinct configurations. The considered structure can undergo a transition from one type of configuration to another during which the Poisson's ratio varies very significantly; without the need to rebuild the system. Namely, the change occurs from a structure possessing a positive Poisson's ratio to a strongly auxetic structure and *vice versa*. In addition, it is shown that a change in the configuration of the system can be used to achieve control over the formation of a phononic band gap. Finally, it is shown that all configurations of the considered system are realizable at the micro-scale, with experimental tests demonstrating a possibility of the reconfiguration of the structure through the use of an external magnetic field.

2 Results and Discussion

In this work, a novel mechanical metamaterial composed of triangle-shaped structural elements is proposed in order to assess its potential to exhibit versatile mechanical and wave propagation properties. As shown in **Fig. 1a**, the considered system can occur in two very different configurations, hereafter referred to as Type A and Type B structures. In the case of the Type A configuration, the system consists of two types of isosceles triangles connected to each other at the vertices. Due to this specific connectivity, the geometry is characterized by three different types of apertures. In contrast, the configuration denoted as Type B has a more regular design and consists of only one type of isosceles triangles. In fact, it resembles a lattice of mutually connected star-shaped elements where each of these elements consists of six triangles. The two configurations were designed in this specific manner in order to ensure that during mechanical deformation they would exhibit very different Poisson's ratios. This concept is depicted schematically in **Fig. 1a**, where qualitatively, Type A and Type B structures exhibit strongly negative

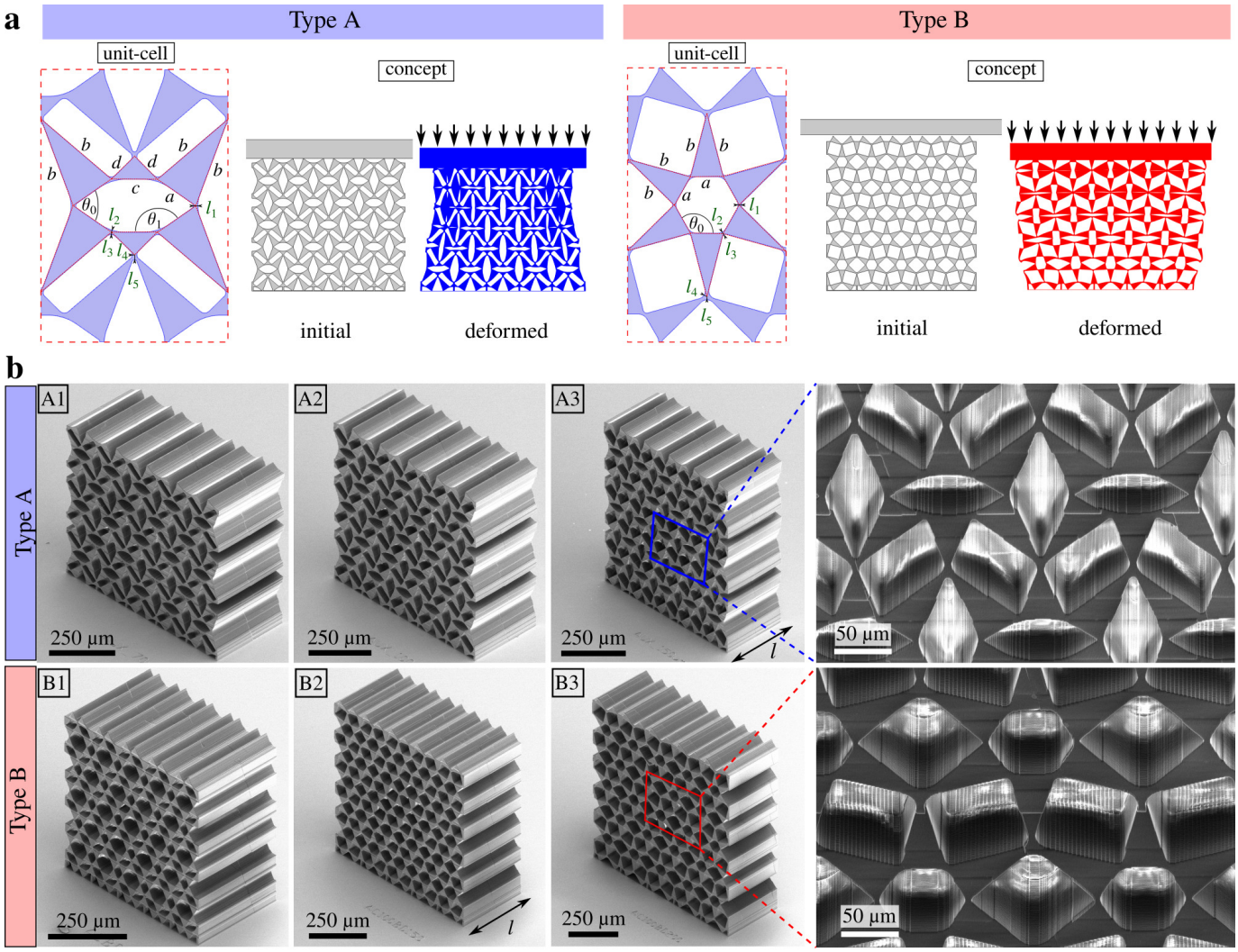

Figure 1: **a)** Diagrams showing the two types of structures considered in this work. **b)** Experimental prototypes corresponding to specific examples of the Type A and Type B structures that are analyzed from the point of view of their mechanical properties. Parameters that remain the same for all structures are the following: $a = 40$ μm, $l_1 = 4.8$ μm, $l_2 = 2.4$ μm, $l_3 = 2.4$ μm, $l_4 = 3.6$ μm, and $l_5 = 6.7$ μm. In addition, parameters that remain the same for type A structures are $b = 80$ μm and $c = 40$ μm. Parameters that assume unique values both for type A and type B systems are as follows: $d = 28$ μm (A1), $d = 40$ μm (A2), $d = 60$ μm (A3) and $b = 40$ μm (B1), $b = 60$ μm (B2), and $b = 80$ μm (B3). The out-of-plane thickness l for all of the structures is equal to 300 μm.

(auxetic behavior) and positive Poisson's ratio, respectively.

In order to investigate the mechanical properties of the two considered configurations and to demonstrate that the proposed concept can be utilized in the case of microscopic applications, experimental prototypes were constructed at the micro-scale (see Methods section). More specifically, as shown in Fig. **1b**, in order to assess the effect of the geometric parameters on the behavior of the structures, three different prototypes were fabricated for each configuration; labeled A1, A2, A3 and B1, B2, B3. In fact, the only difference between the three Type A structures is the value of the d parameter. Similarly, the only difference between the Type B prototypes is the value of the b parameter. All prototypes are composed of 5×3 unit-cells, where the bottom part of the system is clamped as a result of the manufacturing process (see Methods section).

2.1 Mechanical Properties

To determine the Poisson's ratio of the considered systems, the microscopic experimental prototypes were compressed by a flat external indenter along the y-axis, with the bottom part of each sample re-

maining fixed in space. Thus, to qualitatively estimate the Poisson's ratio of the system, one can follow the changes in the horizontal dimension of the topmost part of each structure. More specifically, for all prototypes, the topmost section is unaffected by the bottom constraint due to being very far from the substrate on top of which samples were printed. Hence, the expansion or shrinkage of the x dimension of the fabricated prototypes subjected to the compression along the y-axis indicates the sign of Poisson's ratio. From the optical images of the experiment presented in **Fig. 2a**, one can note from the qualitative analysis that prototypes corresponding to Type A and Type B exhibit very different behaviors. Namely, the x dimension for all the prototypes with a Type A configuration decreases significantly during the compression process which is an indication of strong auxetic behavior. In contrast, for the Type B structures, the horizontal dimension of the samples slightly increases during the deformation process. Such behavior is an indication of a weakly positive Poisson's ratio. This means that Type B configurations exhibit a non-auxetic behavior unlike the Type A samples. At this point, it should be emphasized that the non-uniform deformation of the entire system originates from the fact that the experimental samples remain attached to the substrate after the 3D printing process. However, if one was to consider the deformation of the detached sample, the extent of non-uniformity would be significantly smaller. Nonetheless, mechanical testing could potentially become unreliable in such a scenario due to the very small size of the system. It is also worth emphasizing that if fabricated through the use of appropriate materials, the considered system can maintain its properties over numerous deformation cycles (see **Fig. S1** in the **Supplementary Information**). This, in turn, further enhances its appeal from the perspective of potential applications.

In addition to the qualitative description of the behavior of the system, it is important to conduct a quantitative analysis in order to determine the range of Poisson's ratio values and to assess its usefulness in the case of specific applications. To this aim, in order to calculate the Poisson's ratio for each structure, the central unit-cell was taken into consideration. This stems from the fact that the mechanical behavior of this specific unit-cell is the least affected by edge effects contributing to the uneven deformation pattern. More specifically, the deformation of the central unit-cell is not significantly affected by the bottom part of the system being attached to the substrate. In addition, its behavior is also mostly unaffected by the unbounded left and right-hand sides of the structure as well as any friction imparted through contact of the topmost part of the system with the indenter inducing the deformation. As shown in **Fig. 2b**, all of the Type A structures exhibit strong auxetic behavior throughout the entire deformation process. In fact, the largest extent of auxeticity can be observed for the A3 sample corresponding to the largest value of d. In this case, for a relatively large strain of around 0.07, the Poisson's ratio assumes the value of approximately -1.4. Furthermore, one can note that the extent of auxeticity can be adjusted by the value of d. In contrast, the behavior of the analyzed samples of type B is very different. Namely, all type B samples tend to exhibit a positive Poisson's ratio that in most cases, becomes gradually less positive as strain increases. Notably, the sample that exhibits the largest values of Poisson's ratio throughout the majority of the deformation process is structure B3 that possesses the largest value of b from amongst the considered samples. Thus, taking all of these results into account, there are significant differences between the Poisson's ratios of type A and type B structures. In addition, the range of Poisson's ratio for each configuration can be adjusted through a variation of the geometric parameters.

In addition to experimental studies, another interesting aspect of the analysis corresponds to the investigation of the Poisson's ratio of the system through the FEM (Finite Element Method) computer simulations. In this case, both the structure and the corresponding boundary conditions were designed to closely match the experiment (see Methods section). As shown in **Fig. 2c**, the trends observed for computational results were qualitatively identical to those of the conducted experiments. More specifically, in the case of these two approaches, type A configurations exhibited a strong auxetic behavior throughout the entire deformation process while type B configurations exhibited positive values of this parameter. Of course, in terms of the quantitative analysis, there are some discrepancies between the two approaches that originate from multiple reasons. In the case of the experiment, the effect of the bottom constraint and edge effects on the effective Poisson's ratio is not fully negligible, however it is evident

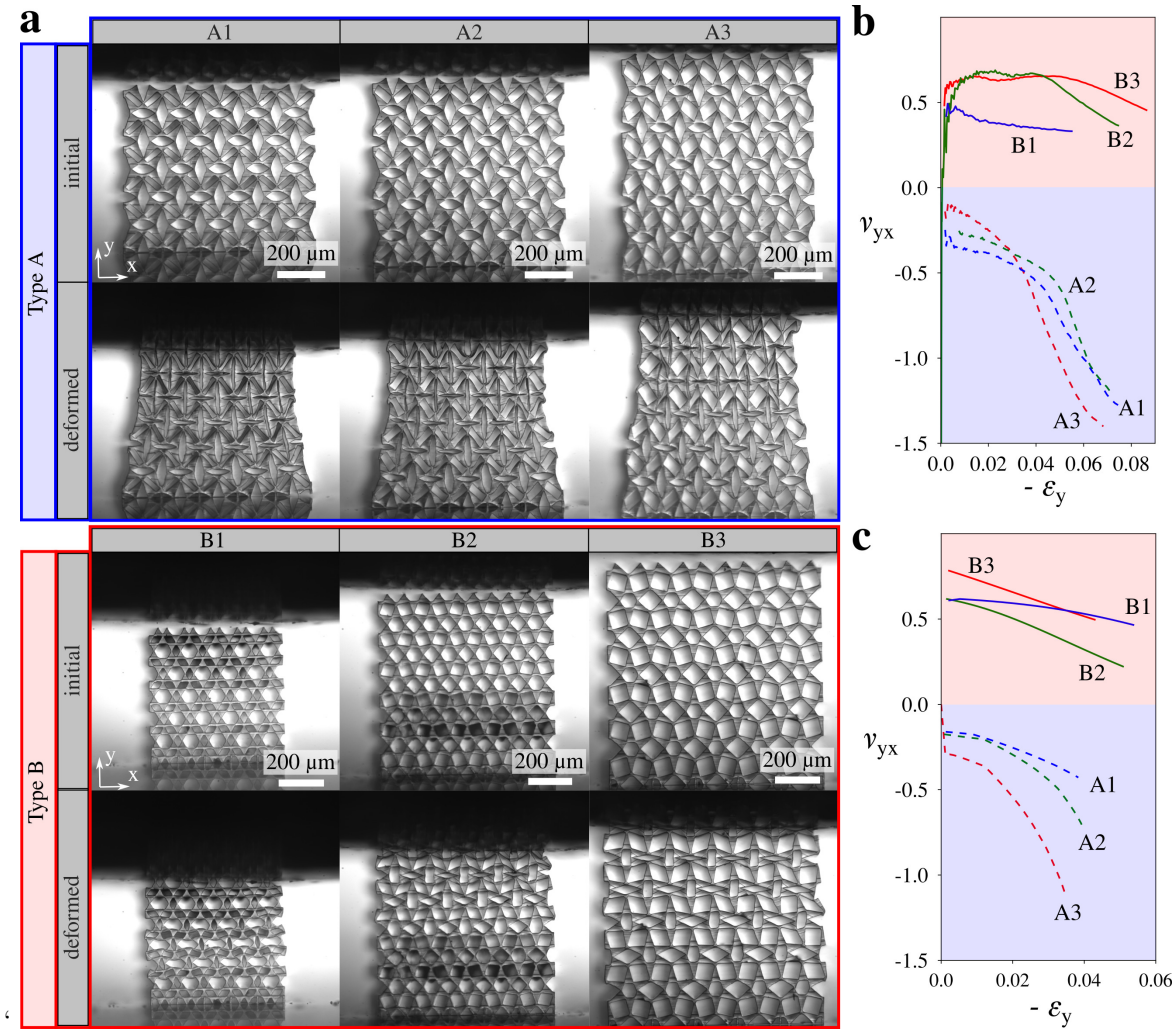

Figure 2: **a)** Optical images of a compression test along the y-axis of the three micro-scale experimental prototypes corresponding to Type A and Type B configurations. **b)** Poisson's ratio estimated from experimental samples. **c)** Poisson's ratio estimated with FEM (Finite Element Method) computer simulations that was calculated based on the deformation of the central unit-cell of the considered finite samples.

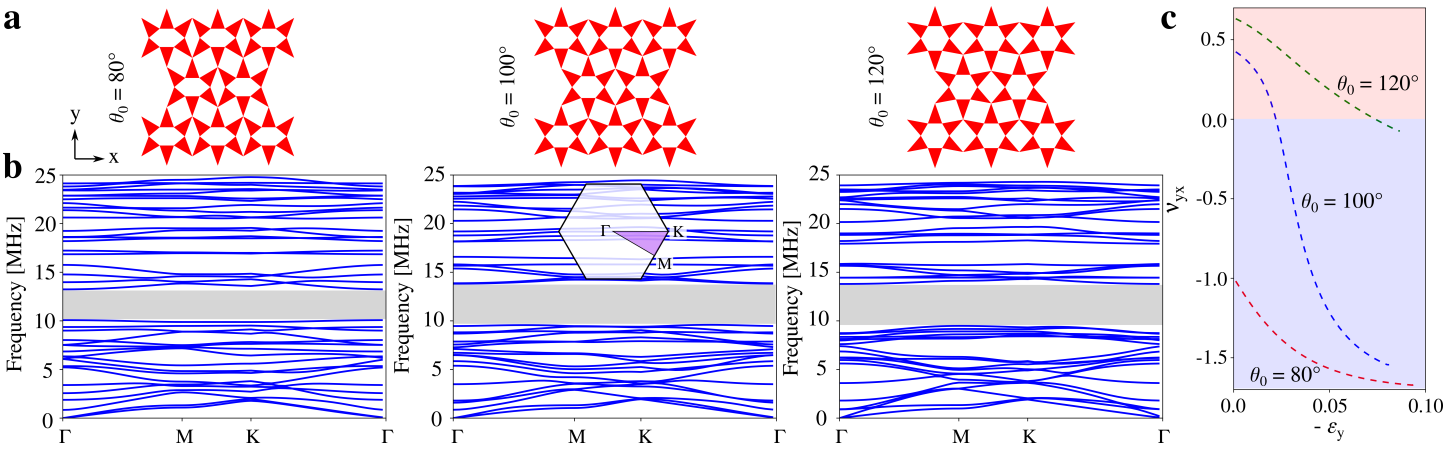

Figure 3: Effect of the reconfiguration of the system on phononic band gap formation and mechanical properties. **a)** Diagrams showing schematically different configurations assumed by the same system. **b)** Phonon dispersion relations for the three considered configurations where the first band gap is highlighted by means of the grey box. **c)** Variation of Poisson's ratio for the three selected structures subjected to mechanical compression along the y-axis. Poisson's ratio was calculated for individual unit-cells with periodic boundary conditions imposed in the x-direction and a symmetric prescribed displacement applied to the topmost and bottommost parts of the system along the y-axis.

that, through the use of multiple cells in the design of the system and the selection of only the central unit-cell for analysis purposes, these influences are certainly significantly diminished. Thus, based on the provided results, it is clear that the two approaches confirm a very significant difference in the Poisson's ratio exhibited by the two types of analyzed configurations.

2.2 Effect of Reconfiguration on the Properties of the Structures

In addition to the Poisson's ratio, another interesting direction of study is the analysis of phononic band gap formation associated with phonon dispersion. Such analysis provides valuable information about the ranges of frequencies for which elastic waves are not transmitted through a given configuration of the system. Hence, in addition to applications related explicitly to a tunable Poisson's ratio, this information can be used for the design of microscopic vibration dampers / sensors.

From the perspective of applications, it is very important to check what happens to the mechanical and wave propagation properties once the system is subjected to a reconfiguration process. In other words, it is essential to assess the properties of the system during a reconfiguration process induced by an external stimulus that does not involve reconstruction of the structure. An example of such a reconfiguration process is presented in **Fig. 3a**, where the initial configuration of type A corresponds to angle $\theta_0 = 80°$. In this case, all triangles are the same and correspond to the $b/a = 1.5$ aspect ratio. Furthermore, as the reconfiguration process begins, the magnitude of the angle θ_0 starts increasing until it reaches the value $\theta_0 = 120°$. At this point, the system assumes a configuration of type B, where there are only two types of apertures. In order to describe what happens to the properties of the system throughout the reconfiguration process, we focus on the three representative configurations depicted schematically in **Fig. 3a**, where θ_0 is equal to 80°, 100° and 120° respectively.

According to **Fig. 3b**, the phononic band structures for all three considered configurations are relatively similar. Most notably, the first non-negligible band gap occurring in the case of the system characterized by $\theta_0 = 80°$ has a size of 2.95 MHz. As the value of θ_0 increases and assumes the values of 100° and 120°, the size of the band gap increases and is equal to 4.03 MHz and 4.13 MHz respectively. However, even though the size of the band gap changes as a result of the reconfiguration process, one could say that such variations are not very significant. This, in turn, is in agreement with the observations made for other complex mechanical metamaterials subjected to a reconfiguration process that were reported in the literature [66]. At this point, it is also important to note that whereas for Fig. 3 a structure cor-

responding to a specific value of the b/a ratio was taken into account, in general, the change in width of the first significant band gap may look different when considering the deformation of structures characterized by different values of b/a. More specifically, as described in the Supplementary Information, if one was to consider the deformation of the structure with $b/a = 2$ from the configuration where $\theta_0 = 80°$ to the configuration corresponding to $\theta_0 = 120°$, the magnitude of the change in the band gap width would be very different from the former case. In this scenario, the relative change in the band gap width is only equal to 0.149 MHz. In contrast, for the structure with $b/a = 1.5$, the change in the band gap width equals 1.18 MHz. Thus, a relatively small variation in the aspect ratio of structural elements may lead to a considerable difference in the magnitude of the change in the width of the band gap during the continuous reconfiguration process. Of course, this is due to the fact that structures corresponding to certain values of b/a lead to considerably different band gaps compared to other systems. Hence, it follows that the change in their magnitude is also considerably different.

Contrary to the results related to band gap formation, it is evident that the reconfiguration process strongly influences the Poisson's ratio of the system. As shown in **Fig. 3c**, configurations associated with $\theta_0 = 80°$ and $\theta_0 = 120°$ assume very different values of Poisson's ratio. Namely, in the case of the system where $\theta_0 = 80°$, the structure exhibits strong auxetic behavior throughout the entire deformation process. On the other hand, for $\theta_0 = 120°$, the value of the Poisson's ratio is predominantly positive. These two results are in accordance with the expectations based on the results of the mechanical testing of different configurations of Type A and Type B. However, it is very interesting to see what happens when the Type A configuration becomes very similar to a Type B configuration. Such a scenario can be observed in the case of the intermediate configuration corresponding to $\theta_0 = 100°$. For this configuration, even though Poisson's ratio is initially positive, it quickly assumes strong negative values upon increasing strain. All of these results are very interesting since they indicate that a relatively simple reconfiguration process of the considered system makes it possible to very significantly change its Poisson's ratio.

Once the effect of the reconfiguration of the system on its properties has been determined, it is also interesting to have a closer look at band gap formation for the Type B system. As shown in **Fig. 3b**, the largest first significant band gap is observed during the reconfiguration process. In order to investigate this factor further, the influence of changing the aspect ratio of the isosceles triangles constituting the Type B structure while keeping the dimension a constant, was analyzed.

The three specific configurations of the system chosen for this analysis are illustrated in **Fig.4a**. In fact, the only difference between them is the value of b. Hence, to refer to a specific configuration assumed by the structure, one can use a particular value of the b/a coefficient. According to **Fig.4b**, the variation in the value of b/a has a very significant effect on the phonon dispersion and on the size of the first significant band gap. More specifically, in the considered range of frequencies, one can note that for the structure associated with $b/a = 0.7$, the first non-negligible band gap is relatively small. In contrast, once the geometric dimensions of the structure are modified to correspond to $b/a = 1.0$, the appearance of a very significant band gap can be observed. Furthermore, upon increasing the magnitude of this coefficient up to a value of 1.3, the size of the first significant band gap is reduced in relation to the configuration with $b/a = 1.0$. This means that at relatively low frequencies, one should expect the largest band gap to be observed for this specific configuration. Hence, as shown in **Fig. 4c**, an analysis of the size of the first three band gaps was conducted for a larger number of possible structures corresponding to the b/a coefficient ranging between 0.7 and 1.3. The results show that the width of the first significant band gap gradually increases until it reaches its maximum value at $b/a = 1.0$. For configurations with b/a exceeding this value, the band gap gradually decreases. Finally, it should be noted that an experimental validation confirming the capability of controlling the width of band gaps through the change in the value of b/a is provided in **Fig. S2** in the **Supplementary Information**.

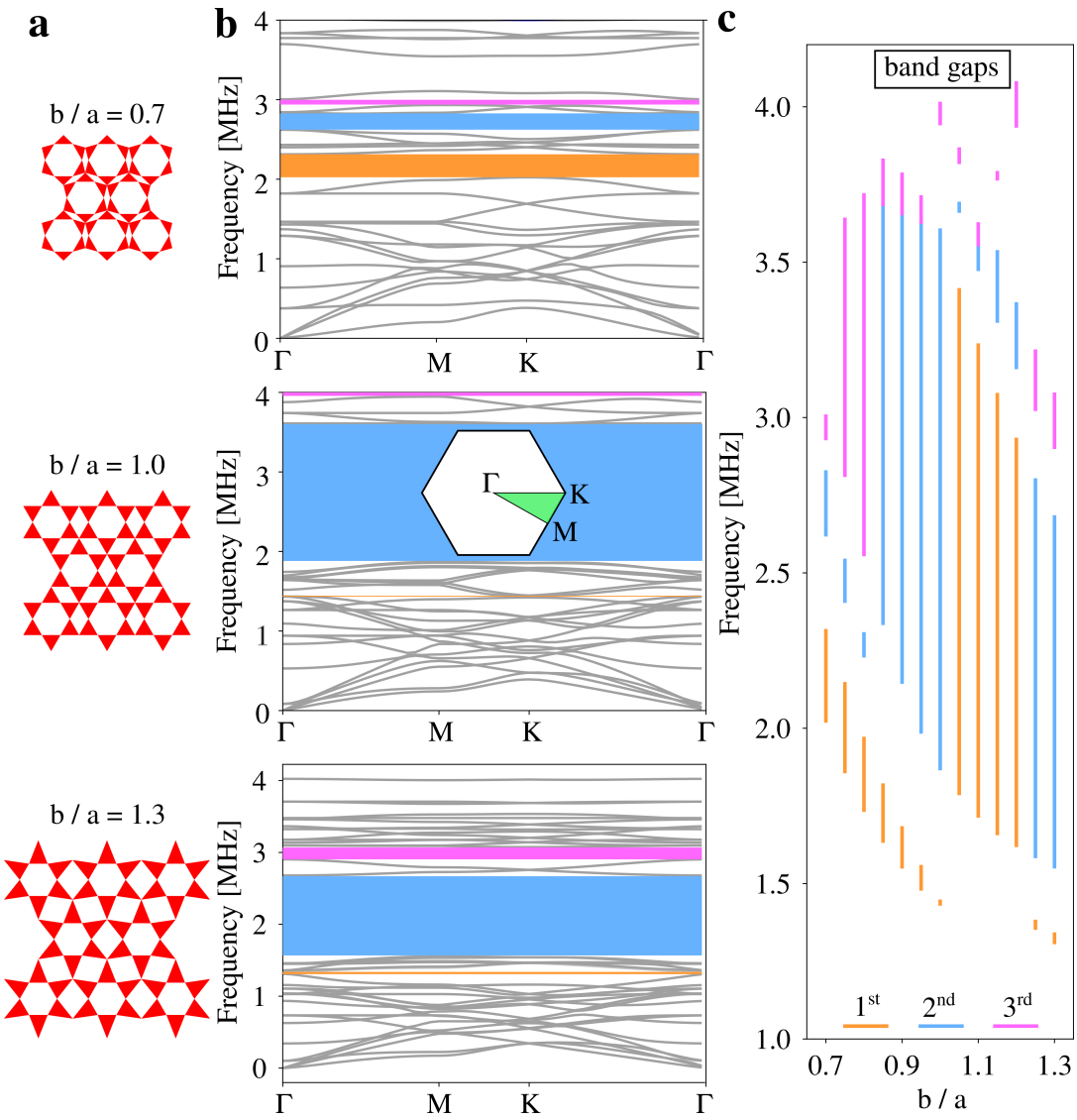

Figure 4: Effect of the elongation of the isosceles triangles corresponding to Type B of the system on the band gap formation. **a)** Diagrams showing three different configurations of the system, where the value of a is kept constant. **b)** Phonon band structures corresponding to the analyzed structures. **c)** The first three band gaps associated with structures corresponding to different values of the b/a ratio. The geometric parameters used for all of the structures were set to be the following: $a = 200$ μm, $l_1 = 8$ μm, $l_2 = 4$ μm, $l_3 = 4$ μm, $l_4 = 4$ μm, $l_5 = 9$ μm

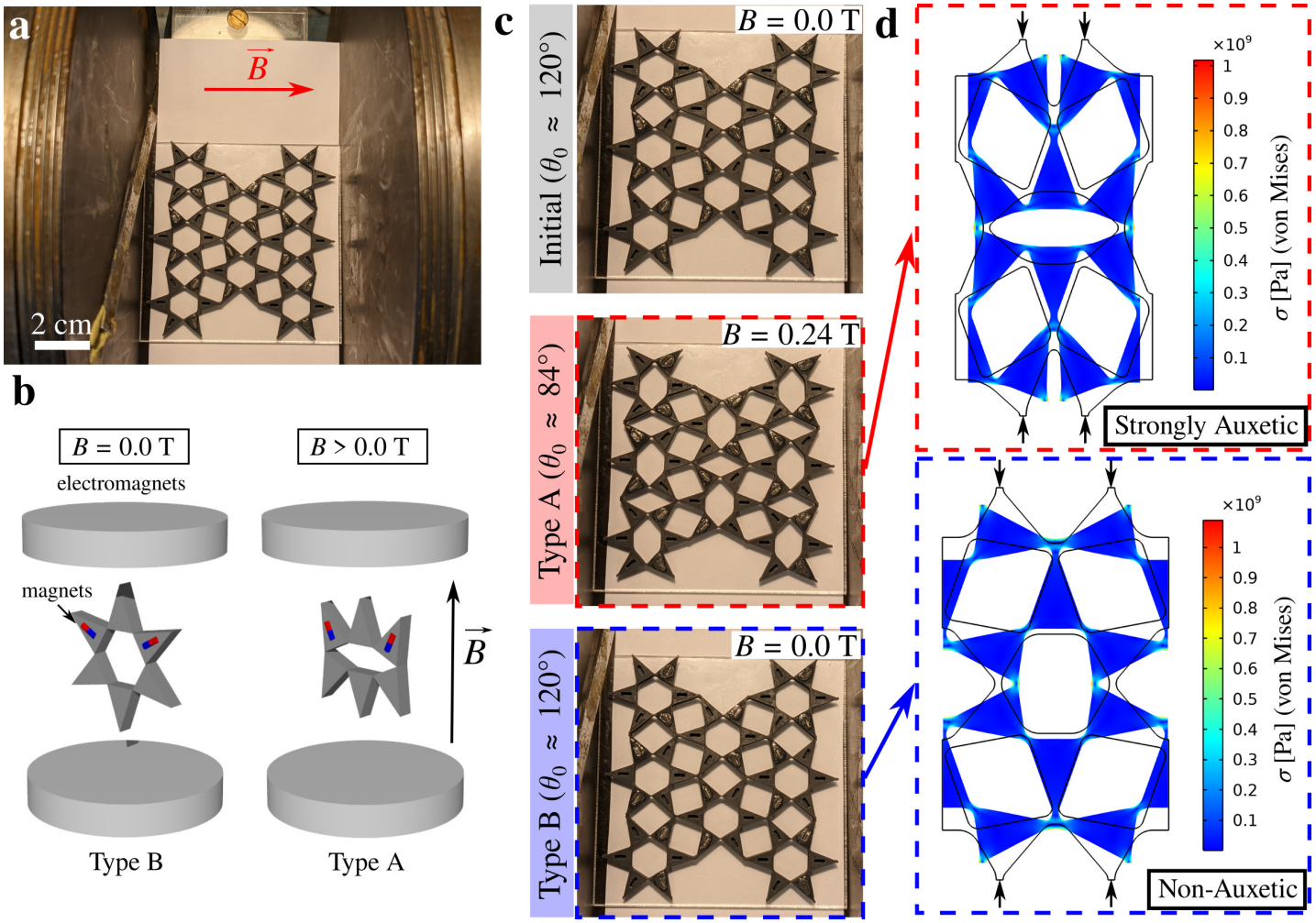

Figure 5: Active reconfiguration and transition in the properties of the system induced by the application of an external magnetic field. **a)** Picture of the investigated sample placed between two parallel electromagnets that produce an approximately uniform magnetic field. **b)** Diagram showing the concept of the reconfiguration of the magneto-mechanical structure. **c)** A change in the configuration of the system induced by the variation in the magnitude of the external magnetic field. **d)** Mechanical deformation of different configurations assumed by the system during the active reconfiguration.

2.3 Active Control

Up to this point, it has been shown that the properties of the proposed mechanical metamaterial can be controlled as a result of the reconfiguration process. However, such reconfiguration was merely a theoretical concept and thus far, it has not been explicitly demonstrated how it could be achieved without reconstructing the system. Thus, in this section, it is demonstrated how such active control over the configuration assumed by the system and the resulting mechanical properties can be attained. Furthermore, since the concept proposed in this work is fully scalable and all results can in general be reproduced irrespective of the size of the system, active control over the reconfiguration process was demonstrated through the use of a macroscopic prototype (see **Fig. 5**).

As shown in **Fig. 5a**, the system selected to demonstrate the active reconfiguration process corresponds to a 3D-printed (see Methods section) prototype associated with the Type B configuration that was inserted into the uniform magnetic field induced by two large parallel electromagnets. The response of the structure to the application of the external magnetic field was made possible due to the use of magnetic inclusions in the form of very small neodymium magnets (see Methods section) that were embedded within some of the structural triangle-like elements constituting the system. The concept of active reconfiguration corresponding to this structure is schematically demonstrated in **Fig. 5b**, where for the sake of clarity, only a fragment of the considered structure is presented. As can be seen, the structure is

initially at rest in the Type B configuration, where $\theta_0 = 120°$. Once the external magnetic field is switched on, the magnetic dipole moments of the magnets attempt to align with the external magnetic field. Of course, depending on the magnitude of the external field, this might not be possible since for the triangles to rotate, the applied torques must be large enough to overcome the resistance and the restoring forces corresponding to the elastic non-magnetic material.

As shown in **Fig. 5c**, the considered structure deforms significantly and assumes a configuration corresponding to $\theta_0 \approx 84°$ upon being subjected to a relatively strong external magnetic field having a magnitude of 0.24 T (see **Supplementary Video 1** to observe the gradual reconfiguration process where the magnetic field was changed with increments of 0.01 T). In other words, the structure undergoes a transition from Type B to Type A configuration. Based on the computational results provided in **Fig. 5d**, one can note that these two configurations correspond to a very different Poisson's ratio. Thus, the application of the external magnetic field makes it possible to significantly modify the properties of the structure without the need to rebuild it. In addition, after switching off the external magnetic field, the structure returns to its initial configuration, which means that after the transition it is possible to recover the initial properties of the system. These results are very important as they prove that the mechanical metamaterial proposed in this work can be used to exhibit a versatile Poisson's ratio that can be controlled remotely via the magnitude and orientation of the external magnetic field. Of course, in this case, due to the scale of the prototype, the controllable behavior was achieved thanks to the use of magnetic inclusions in the form of neodymium magnets. However, at much lower scales, this approach should be replaced for example by the use of single domain superparamagnetic nanoparticles dispersed within the resin prior to the polymerization process [69, 70]. Another approach that could be used to achieve control over the behavior of the system through the use of an external magnetic field, is to use a selective magnetic coating applied for example by sputtering following the 3D printing fabrication process [71, 72]. At this point, we emphasize that the results of this work are scale independent. Depending on the size of the system, however, they can be better suited for specific applications.

The results show that the proposed system can exhibit two very useful properties at the same time that are controllable remotely via an applied external magnetic field without the need for reconstructing the system. Specifically, it was shown that the considered structure can undergo a transition from positive to highly negative Poisson's ratio solely as a result of a reconfiguration process that can be invoked and controlled remotely. In addition, after the transition, the system maintains a stable mechanical behaviour for relatively large strains. Such active and reversible control over mechanical properties, combined with the observation of a very significant variation of Poisson's ratio, is seldom observed in mechanical metamaterials and can be very useful for numerous applications. Furthermore, what makes these results even more appealing, is the fact that it is demonstrated that the highly versatile Poisson's ratio of the considered system can be observed for samples fabricated at the micro-scale. In addition, from the perspective of multifunctional devices, the proposed system exhibits two highly useful properties at once: controllable Poisson's ratio and adjustable phononic band gap. The latter property prevents waves in a specific range of frequencies from propagating through the system. Mechanical metamaterials exhibiting such band gap formation combined with fully controllable Poisson's ratio are extremely rare. In a few known instances where control over both aspects was attempted to some extent [56], the studies were limited to structures at the macro / millimetre scale and typically only one of these properties was quantitatively assessed.

As mentioned above, the reconfiguration process leading to the transition in the properties of the system is fully reversible and can be achieved in an active manner that does not require rebuilding the system. This means that the ability of the mechanical metamaterial to exhibit a tunable Poisson's ratio could be used at the macroscale or the millimeter scale in the design of smart protective devices that could adjust their mechanical response depending on the specific impacting body, e.g. active car bumpers. Similarly, at the microscale, the controllable Poisson's ratio can lead to the design of materials characterized by the programmable extent of their micro-indentation resistance. In addition, should somebody use magnetic inclusions to control the properties of the structure, then by distributing them in a non-uniform

manner, it would be possible to observe a situation where the initially uniformly-designed structure exhibits a very different Poisson's ratio in different parts of the system. Such behavior, as demonstrated in another study [64], could enable the system to exhibit complex shape morphing upon being subjected to a mechanical deformation or through the application of an external magnetic field. Especially at the micro-scale, and among other applications, such shape morphing may be useful for the design of smart stents that would provide local support to specific parts of a blood vessel, where the location of the support could be changed throughout treatment. Finally, it was also demonstrated that in addition to control over the Poisson's ratio, one can form band gaps that are almost unaffected by the reconfiguration process. Thus, while changing the mechanical response of the sample, it would be possible to prevent waves corresponding to a specific range of frequencies from being transmitted through the system. Such ability could be very interesting from the perspective of the design of multifunctional vibration-damping protective devices. Alternatively, should the need arise, the band gap could be adjusted by a variation in geometric parameters of the system. In addition, for specific values of the b/a parameter, the change in the width of the band gap induced by mechanical deformation is considerable.

3 Conclusion

In this work, a novel micro-scale mechanical metamaterial was proposed. It was demonstrated that depending on the assumed configuration, the system can exhibit very different Poisson's ratios ranging from strongly negative to positive values at relatively large strains. In addition, it was shown that such control over the mechanical behavior of the system can be achieved as a result of active reconfiguration, i.e. a process that does not require rebuilding the system. The transiton of properties of the structure following the reconfiguration process is recoverable and the extent of changes can be controlled by means of an external stimulus, such as a magnetic field. Furthermore, in addition to control over Poisson's ratio, it was demonstrated that during the reconfiguration process one can approximately retain the band gap formation corresponding to the system. Alternatively, band gap formation can be also tailored by an appropriate variation in the geometric parameters. All of these results indicate that the proposed mechanical metamaterial can be very useful in a plethora of applications ranging from smart protective to biomedical devices.

4 Methods

4.1 Fabrication

The Poisson's ratio of the considered system was assessed based on micro-scale experimental prototypes produced through the use of a commercial 3D printer (Photonic Professional GT+, Nanoscribe GmbH). The 3D printer used in this work operates based on the two-photon lithography method. All samples were printed with a resolution of around 2 μm which was possible thanks to use of the negative tone IP-S photoresin (Nanoscribe GmbH). Prior to the printing process, a drop of resin was deposited on an ITO-coated soda-lime glass substrate having the following dimensions: $25 \times 25 \times 0.7$ mm^3. After deposition, specific fragments of the drop were photopolymerized by means of a 25X-objective with a femtosecond laser that was operating at $\lambda = 780$ nm. Furthermore, the standard printing parameters were set as follows: a galvanometric scanning speed of 100 mm/s, a laser power at the level of 90% and slicing as well as hatching distances equal to 1 μm and 0.5 μm respectively. Once the printing process was finished, each sample was developed for 25 min in a solution of PGMEA (Propylene Glycol Methyl Ether acetate). This step of the procedure allows to remove the nonpolymerized photoresist. Subsequently, the resulting structure was rinsed for a duration of three minutes in isopropyl alcohol (IPA) in order to remove the developer solution.

In the case of the macroscopic experimental prototype, the structure was 3D printed by means of a commercial FDM 3D-printer (Ultimaker) by means of the elastic TPU 95A material. Furthermore, in each of the star-shaped segments of the structure, there were two apertures with magnetic inclusions in the form

of 3 neodymium magnets of the N42 type. Each of the magnets had a cylindrical shape with a height of 1 mm and a base diameter equal to 1 mm. The remanent induction of each magnet was estimated to be equal to 0.613 T. The geometric dimensions of the initial structure were set to be the following: $a = 6$ mm, $b = 9$ mm, $l_1 = 0.7$ mm, $l_2 = 0.43$ mm, $l_3 = 0.36$ mm, $l_4 = 0.8$ mm and $l_5 = 0.55$ mm.

4.2 Mechanical Compression Testing

The experimental samples considered in this work were tested mechanically in order to assess their Poisson's ratio. To this aim, all samples were subjected to a mechanical compression induced by a flat external indenter. The speed of the indenter was constant and was set to 1 μm s^{-1}. At the same time, the bottom part of each sample was fixed in place by adhesion to the substrate on top of which they were printed. Throughout the experiment, the deformation process was recorded by means of an optical camera with magnification factor x20. The working distance, i.e. the distance between the lens of the camera and the sample, was approximately equal to 11 mm. Based on the recorded pictures, the Poisson's ratio of the system was determined based on the central topmost unit-cell (see **Supplementary Information**). To track the position of vertices that could be used to calculate the Poisson's ratio of the selected unit-cell, the digital image correlation method implemented in the MATLAB software was used.

In the case of the results presented in **Fig. 5**, the macroscopic experimental prototype was inserted into the uniform external magnetic field that was induced by two parallel electromagnets. The magnitude of the applied field was varied in a range between 0 T and 0.24 T with steps of 0.01 T in order to induce the reconfiguration process (see **Supplementary Video 1**). The deformation of the structure was recorded by means of a standard optical camera.

4.3 FEM simulations

To determine the Poisson's ratio of the considered finite structurs resembling experimental prototypes presented in **Fig. 2**, FEM simulations were conducted by means of the commercial software COMSOL Multiphysics. To this aim, for each of the structures considered in **Fig. 2**, it was assumed that geometric parameters characterizing the structure are the same as in the case of the experimental samples. Furthermore, to match the boundary conditions used in the experiments, it was assumed that the bottom part of each of the systems is fixed in space. In addition, the deformation of the structure was induced by means of contact with a large flat indenter in order to match the deformation process observed in the experiments as closely as possible. Mechanical properties of the simulated material were set as $E = 4$ GPa, $\nu = 0.4$ and $\rho = 1200$ kg m^{-3}. In addition, geometrical nonlinearities were implemented to make simulations more realistic under large strains. Finally, it should be emphasized that a specific method related to the calculation of the Poisson's ratio is provided in the **Supplementary Information**.

In order to determine the phonon band structure, Bloch boundary conditions were implemented and used via an eigenvalue solver assuming real wave vectors in the Bloch conditions and searching for real eigenfrequencies of the system.

Supporting Information
Supporting Information is available from the Wiley Online Library or from the corresponding author upon request.

Acknowledgements
This work was partly supported by the french RENATECH network and its FEMTO-ST technological facility.
K.K.D. acknowledges the support of the Polish National Science Centre (NCN) in the form of the grant awarded as a part of the SONATINA 5 program, project No. 2021/40/C/ST5/00007 under the name "Programmable magneto-mechanical metamaterials guided by the magnetic field".

This research was funded by the Polish Minister of Education and Science under the program "Regional Initiative of Excellence" in 2019-2023, project No. 003/RID/2018/19, funding amount PLN 11 936 596.10.

References

[1] B. Florijn, C. Coulais, M. van Hecke, *Phys. Rev. Lett.* **2014**, *113,* 175503.

[2] C. Coulais, E. Teomy, K. de Reus, Y. Shokef, M. van Hecke, *Nature* **2016**, *535,* 529.

[3] C. Coulais, A. Sabbadini, F. Vink, M. van Hecke, *Nature* **2018**, *561,* 512.

[4] R. Fleury, D. L. Sounas, C. F. Fleck, M. R. Haberman, A. Alú, *Science* **2014**, *343,* 516.

[5] R. Fleury, D. L. Sounas, A. Alú, *Nat. Commun.* **2015**, *6,* 5905.

[6] F. Wenz, I. Schmidt, A. Leichner, T. Lichti, S. Baumann, H. Andrae, C. Eberl, *Adv. Mater.* **2021**, *33,* 2008617.

[7] Y. Zhu, M. Birla, K. R. Oldham, E. T. Filipov, *Adv. Funct. Mater.* **2020**, *30,* 2003741.

[8] T.-Y. Huang, H.-W. Huang, D. D. Jin, Q. Y. Chen, J. Y. Huang, L. Zhang, H. L. Duan, *Sci. Adv.* **2020**, *6,*.

[9] H. Tao, J. Gibert, *Adv. Funct. Mater.* **2020**, *30,* 2001720.

[10] J. A. Jackson, M. C. Messner, N. A. Dudukovic, W. L. Smith, L. Bekker, B. Moran, A. M. Golobic, A. J. Pascall, E. B. Duoss, K. J. Loh, C. M. Spadaccini, *Sci. Adv.* **2018**, *4,* eaau6419.

[11] J. Qi, Z. Chen, P. Jiang, W. Hu, Y. Wang, Z. Zhao, X. Cao, S. Zhang, R. Tao, Y. Li, D. Fang, *Adv. Sci.* **2021**, 2102662.

[12] H. M. A. Kolken, S. Janbaz, S. M. A. Leeflang, K. Lietaert, H. H. Weinans, A. A. Zadpoor, *Mater. Horiz.* **2018**, *5,* 28.

[13] T. van Manen, S. Janbaz, K. M. B. Jansen, A. A. Zadpoor, *Commun. Mater.* **2021**, *2,* 56.

[14] M. Miniaci, A. Krushynska, F. Bosia, N. M. Pugno, *New J. Phys.* **2016**, *8,* 083041.

[15] G. Imbalzano, P. Tran, T. D. Ngo, P. V. S. Lee, *Compos. Struct.* **2016**, *135,* 339.

[16] N. Novak, M. Borovinsek, O. Al-Ketan, Z. Ren, M. Vesenjak, *Compos. Struct.* **2022**, *300,* 116174.

[17] O. Duncan, T. Shepherd, C. Moroney, L. Foster, P. D. Venkatraman, K. Winwood, T. Allen, A. Alderson, *Appl. Sci.* **2018**, *8,* 941.

[18] A. Russo, B. Y. Ahn, J. J. Adams, E. B. Duoss, J. T. Bernhard, J. A. Lewis, *Adv. Mater.* **2011**, *23,* 3426.

[19] S. Huang, Y. Liu, Y. Zhao, Z. Ren, C. F. Guo, *Adv. Funct. Mater.* **2019**, *29,* 1805924.

[20] R. Lakes, *Science* **1987**, *235,* 1038.

[21] K. E. Evans, A. Alderson, *Adv. Mater.* **2000**, *12,* 617.

[22] A. S. Gladman, E. A. Matsumoto, R. G. Nuzzo, L. Mahadevan, J. A. Lewis, *Nat. Mater.* **2016**, *15,* 413.

[23] J. T. B. Overvelde, J. C. Weaver, C. Hoberman, K. Bertoldi, *Nature* **2017**, *541,* 347.

[24] M. J. Mirzaali, S. Janbaz, M. Strano, L. Vergani, A. A. Zadpoor, *Sci. Rep.* **2018**, *8,* 965.

[25] J. L. Silverberg, A. A. Evans, L. McLeod, R. C. Hayward, T. Hull, C. D. Santangelo, I. Cohen, *Science* **2014**, *345,* 647.

[26] A. Rafsanjani, K. Bertoldi, A. R. Studart, *Sci. Robot.* **2019**, *4,* eaav7874.

[27] P. Cai, C. Wang, H. Gao, X. Chen, *Adv. Mater.* **2021**, *33,* 2007977.

[28] C. Song, B. Zou, Z. Cui, Z. Liang, J. Ju, *Adv. Funct. Mater.* **2021**, *31,* 2101395.

[29] S. Li, G. Librandi, Y. Yao, A. J. Richard, A. Schneider-Yamamura, J. Aizenberg, K. Bertoldi, *Adv. Mater.* **2021**, *33,* 2105024.

[30] K. Bertoldi, V. Vitelli, J. Christensen, M. van Hecke, *Nat. Rev. Mater.* **2017**, *2,* 17066.

[31] J. N. Grima, R. Gatt, B. Ellul, E. Chetcuti, *J. Non. Cryst. Solids* **2010**, *356,* 1980.

[32] R. M. Neville, F. Scarpa, A. Pirrera, *Sci. Rep.* **2016**, *6,* 31067.

[33] X. Chen, J. Moughames, Q. Ji, J. A. I. Martínez, H. Tan, S. Adrar, N. Laforge, J.-M. Cote, S. Euphrasie, G. Ulliac, et al., *Extreme Mechanics Letters* **2020**, *41* 101048.

[34] X. Chen, Q. Ji, J. A. I. Martinez, H. Tan, G. Ulliac, V. Laude, M. Kadic, *Journal of the Mechanics and Physics of Solids* **2022**, *167* 104957.

[35] X. Tan, J. A. I. Martínez, G. Ulliac, B. Wang, L. Wu, J. Moughames, M. Raschetti, V. Laude, M. Kadic, *Small* **2022**, *18*, 28 2202128.

[36] X. Chen, J. Moughames, Q. Ji, J. A. I. Martínez, H. Tan, G. Ulliac, V. Laude, M. Kadic, *Journal of the Mechanics and Physics of Solids* **2022**, *169* 105057.

[37] B. Deng, A. Zareei, X. Ding, J. C. Weaver, C. H. Rycroft, K. Bertoldi, *Adv. Mater.* **2022**, *34,* 2206238.

[38] K. W. Wojciechowski, *Phys. Lett. A* **1989**, *137,* 60.

[39] L. Mizzi, K. M. Azzopardi, D. Attard, J. N. Grima, R. Gatt, *Phys. Status Solidi RRL* **2015**, *9,* 425.

[40] Y.-L. Wei, Q.-S. Yang, R. Tao, *Int. J. Mech. Sci.* **2021**, *195,* 106267.

[41] L. Wang, G. Ulliac, B. Wang, J. A. I. Martinez, K. K. Dudek, V. Laude, M. Kadic, *Adv. Sci.* **2022**, 2204721.

[42] J. Qu, M. Kadic, M. Wegener, *Applied Physics Letters* **2017**, *110*, 17 171901.

[43] T. A. M. Hewage, K. L. Alderson, A. Alderson, F. Scarpa, *Adv. Mater.* **2016**, *28,* 10323.

[44] K. K. Dudek, R. Gatt, J. N. Grima, *Mater. Des.* **2020**, *187,* 108403.

[45] X. Tan, L. Wang, S. Zhu, S. Chen, B. Wang, M. Kadic, *Eur. J. Mech. A Solids* **2022**, *96,* 104702.

[46] J. Qu, M. Kadic, M. Wegener, *Extreme Mechanics Letters* **2018**, *22* 165.

[47] Z. G. Nicolaou, A. E. Motter, *Nat. Mater.* **2012**, *11,* 608.

[48] R. H. Baughman, S. Stafstrom, C. Cui, S. O. Dantas, *Science* **1998**, *279,* 1522.

[49] T. Li, F. Liu, L. Wang, *Compos. B. Eng.* **2020**, *198,* 108229.

[50] S. Yuan, C. K. Chua, K. Zhou, *Adv. Mater. Technol.* **2019**, *4,* 1800419.

[51] M. Mohsenizadeh, F. Gasbarri, M. Munther, A. Beheshti, K. Davami, *Mater. Des.* **2018**, *139,* 521.

[52] A. O. Krushynska, M. Miniaci, F. Bosia, N. M. Pugno, *Extreme Mech. Lett.* **2017**, *12,* 30.

[53] J. N. Grima, R. Caruana-Gauci, M. R. Dudek, K. W. Wojciechowski, R. Gatt, *Smart Mater. Struct.* **2013**, *22,* 084016.

[54] R. Galea, K. K. Dudek, P.-S. Farrugia, L. Z. Mangion, J. N. Grima, R. Gatt, *Compos. Struct.* **2022**, *280,* 114921.

[55] M. Pishvar, R. L. Harne, *Adv. Sci.* **2020**, *7,* 2001384.

[56] S. M. Montgomery, S. Wu, X. Kuang, C. D. Armstrong, C. Zemelka, Q. Ze, R. Zhang, R. Zhao, H. H. J. Qi, *Adv. Funct. Mater.* **2021**, *31,* 2005319.

[57] C. Ma, Y. Chang, S. Wu, R. R. Zhao, *ACS Appl. Mater. Interfaces* **2022**, *14,* 33892.

[58] Q. Ji, J. Moughames, X. Chen, G. Fang, J. J. Huaroto, V. Laude, J. A. I. Martinez, G. Ulliac, C. Clevy, P. Lutz, K. Rabenorosoa, V. Guelpa, A. Spangenberg, J. Liang, A. Mosset, M. Kadic, *Commun. Mater.* **2021**, *2,* 93.

[59] R. Gatt, L. Mizzi, J. I. Azzopardi, K. M. Azzopardi, D. Attard, A. Casha, J. Briffa, J. N. Grima, *Sci. Rep.* **2015**, *5,* 8395.

[60] Y. Cho, J.-H. Shin, A. Costa, V. K. T. A. Kim, J. Li, S. Y. Lee, S. Yang, H. N. Han, I.-S. Choi, D. J. Srolovitz, *Proc. Natl. Acad. Sci.* **2014**, *111,* 17390.

[61] Y. Tang, G. Lin, L. Han, S. Qiu, S. Yang, J. Yin, *Adv. Mater.* **2015**, *27,* 7181.

[62] N. An, A. G. Domel, J. Zhou, A. Rafsanjani, K. Bertoldi, *Adv. Funct. Mater.* **2020**, *30,* 1906711.

[63] K. Billon, I. Zampetakis, F. Scarpa, M. Ouisse, E. Sadoulet-Reboul, M. Collet, A. Perriman, A. Hetherington, *Compos. Struct.* **2017**, *160,* 1042.

[64] K. K. Dudek, J. A. I. Martínez, G. Ulliac, M. Kadic, *Adv. Mater.* **2022**, *34,* 2110115.

[65] K. K. Dudek, J. A. I. Martínez, M. Kadic, *Phys. Status Solidi B* **2022**, 2200404.

[66] V. Kunin, S. Yang, Y. Cho, P. Deymier, D. J. Srolovitz, *Extreme Mech. Lett.* **2016**, *6,* 103.

[67] T. Frenzel, J. Köpfler, E. Jung, M. Kadic, M. Wegener, *Nat. Commun.* **2019**, *10,* 3384.

[68] C. Mei, L. Li, H. Tang, X. Han, X. Wang, Y. Hu, *Compos. Struct.* **2021**, *271,* 114118.

[69] H.-W. Huang, M. S. Sakar, A. J. Petruska, S. Pane, B. J. Nelson, *Nat. Commun.* **2016**, *7* 12263.

[70] J. Kim, S. E. Chung, S.-E. Choi, H. Lee, J. Kim, S. Kwon, *Nature Mater.* **2011**, *10* 747.

[71] T.-Y. Huang, M. S. Sakar, A. Mao, A. J. Petruska, F. Qiu, X.-B. Chen, S. Kennedy, D. Mooney, B. J. Nelson, *Adv. Mater.* **2015**, *27* 6644.

[72] J. Cui, T.-Y. Huang, Z. Luo, P. Testa, H. Gu, X.-Z. Chen, B. J. Nelson, L. J. Heyderman, *Nature* **2019**, *575* 164.